Article

Laminated Morphology of Nontwisting β-Sheet Fibrils Constructed via Peptide Self-Assembly

Matthew S. Lamm, Karthikan Rajagopal, Joel P. Schneider, and Darrin J. Pochan

J. Am. Chem. Soc., **2005**, 127 (47), 16692-16700• DOI: 10.1021/ja054721f • Publication Date (Web): 05 November 2005

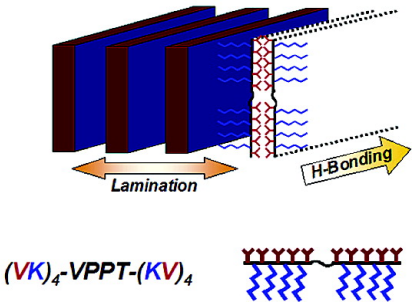

More About This Article

Additional resources and features associated with this article are available within the HTML version:

- Supporting Information
- Links to the 14 articles that cite this article, as of the time of this article download
- Access to high resolution figures
- Links to articles and content related to this article
- Copyright permission to reproduce figures and/or text from this article

View the Full Text HTML

J|A|C|S
ARTICLES
Published on Web 11/05/2005

Laminated Morphology of Nontwisting β-Sheet Fibrils Constructed via Peptide Self-Assembly

Matthew S. Lamm,[†] Karthikan Rajagopal,[‡] Joel P. Schneider,*[,‡] and Darrin J. Pochan*[,†]

Contribution from the Department of Materials Science and Engineering, the Delaware Biotechnology Institute, and the Department of Chemistry and Biochemistry, University of Delaware, Newark, Delaware 19716

Received July 14, 2005; E-mail: pochan@udel.edu; schneijp@udel.edu

Abstract: A synthetic peptide has been de novo designed that self-assembles into β-sheet fibrils exhibiting a nontwisted, stacked morphology. The stacked morphology is constituted by 2.5 nm wide filaments that laterally associate to form flat fibril laminates exceeding 50 nm in width and micrometers in length. The height of each fibril is limited to the length of exactly one peptide monomer in an extended β-strand conformation, approximately 7 nm. Once assembled, these highly ordered, 2-D structures are stable over a wide range of pH and temperature and exhibit characteristics similar to those of amyloid fibrils. Furthermore, the rate of assembly and degree of fibril lamination can be controlled with kinetic parameters of pH and temperature. Finally, the presence of a diproline peptide between two β-sheet-forming strands in the peptide sequence is demonstrated to be an important factor in promoting the nontwisting, laminated fibril morphology.

Introduction

The ability of peptides and proteins to adopt specific secondary, tertiary, and quaternary structures provides unique opportunities for design of nanoscale materials that are not easily available with traditional organic molecules and polymers.[1] In addition, the variety of chemical functionality available via naturally occurring and nonnatural amino acids, in combination with the ability to exactly sequence these functionalities, provides possibilities for the construction of nanomaterials with ultimate desired structure and chemical function. In nature, protein chemical and conformational specificity is utilized for construction of extraordinary materials ranging from rigid, biomineralized shells and bones[2] to high-strength spider silks.[3] Inspired by those extraordinary natural materials, we have designed short peptides that self-assemble into β-sheet fibrils for potential applications ranging from tissue engineering to hybrid bioinorganic nanomaterials. Furthermore, we have begun to investigate the relationship between peptide design, the resultant conformation, and morphological properties of the self-assembled peptide with the intent of uncovering paradigms that can be used for rational peptide design with desired consequent supramolecular structure and function. We have found that insertion of two proline amino acids between two β-sheet-forming peptide strands, composed primarily of alternating valine and lysine residues, results in a self-assembled fibrillar nanostructure with a nontwisted, laminated morphology. The rate of assembly can be tuned with pH and temperature and used to affect the degree of fibril lamination.

Currently, there are many examples of β-sheet fibrillar assemblies from both naturally occurring proteins as well as de novo designed peptides. Much of this work has been performed in the context of amyloid and prion disease states, such as Alzheimer's, Huntington's, type II Diabetes, Creutzfeldt−Jakob disease, etc., and are characterized by the misfolding and self-assembly of native proteins into β-sheet fibrils.[4] Extensive research has focused primarily on understanding the factors that lead to amyloid formation such as protein sequence, environmental conditions, and their relationship to the physiological and neurodegenerative disorders. The structures of many amyloid fibrils have been well characterized using techniques including solid-state NMR and X-ray diffraction, although the exact mechanism of fibril formation remains unclear.[5−7] In addition to naturally occurring amyloid proteins, researchers have studied a variety of other β-sheet fibril-forming motifs derived from amyloid protein fragments, de novo designed peptides, peptidomimetics, and peptide amphiphiles. Lynn and co-workers have studied and characterized the 26 amino acid fragment A$\beta_{(10-35)}$ of the Alzheimer's amyloid protein and used

[†] Department of Materials Science and Engineering, the Delaware Biotechnology Institute.
[‡] Department of Chemistry and Biochemistry.

(1) Rajagopal, K.; Schneider, J. P. *Curr. Opin. Struct. Biol.* **2004**, *14*, 480−486.
(2) Mann, S. *Biomineralization: Principles and Concepts in Bioinorganic Materials Chemistry*; Oxford University Press: Oxford, 2001.
(3) *The Mechanical Properties of Biological Materials*; Vincent, J. F., Currey, J. D., Eds.; Cambridge University Press: Cambridge, 1980.
(4) Kelly, J. W. *Curr. Opin. Struct. Biol.* **1996**, *6*, 11−17.
(5) Jaroniec, C. P.; MacPhee, C. E.; Bajaj, V. S.; McMahon, M. T.; Dobson, C. M.; Griffin, R. G. *Proc. Natl. Acad. Sci. U.S.A.* **2004**, *101*, 711−716.
(6) Petkova, A. T.; Ishii, Y.; Balbach, J. J.; Antzutkin, O. N.; Leapman, R. D.; Delaglio, F.; Tycko, R. *Proc. Natl. Acad. Sci. U.S.A.* **2002**, *99*, 16742−16747.
(7) Sunde, M.; Serpell, L. C.; Bartlam, M.; Fraser, P. E.; Pepys, M. B.; Blake, C. C. F. *J. Mol. Biol.* **1997**, *273*, 729−739.

10.1021/ja054721f CCC: $30.25

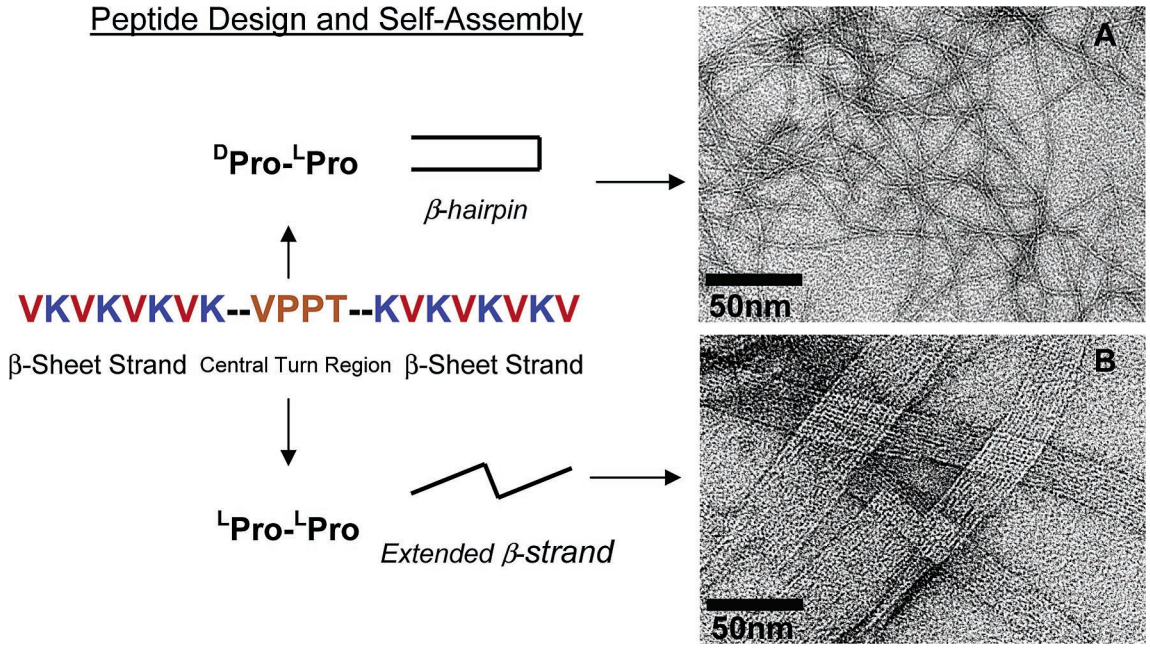

Figure 1. Effect of turn sequence on peptide conformation and self-assembled material. Peptides with DPro-LPro in the central turn region adopt a β-hairpin conformation and reversibly self-assemble into β-sheet-rich hydrogels, whereas peptides with LPro-LPro in the central region adopt an extended peptide conformation and assemble into irreversible, amyloid-like fibril precipitates. (A) TEM of negatively stained hydrogel of $(VK)_4-V^DPPT-(KV)_4$ revealing entangled fibrils each 3 nm wide. (B) TEM of negatively stained precipitates showing the highly laminated, ribbonlike morphology of $(VK)_4-VPPT-(KV)_4$ fibrils.

it to construct peptide fibrils and nanotubes.[8−10] Agelli, Boden, Messersmith, and Zhang have used de novo designed peptides to assemble a range of fibril morphologies ranging from helical ribbons to twisted fibrils.[11−15] Kelly's group has used peptidomimetics to assemble fibrils of varying morphology.[16] Stupp's group has self-assembled peptide amphiphiles[17] containing β-sheet-forming amino acids for cell differentiation[18] and inorganic growth.[19,20] There still remains much to learn about the design and self-assembly of peptides; specifically, the relationship between peptide primary structure and the consequent morphology of the self-assembled nanostructure, i.e., filamentous versus laminated and twisted versus nontwisted.

Previous research by our groups has investigated the importance of peptide design in determining the mechanism of self-assembly and consequent supramolecular structure. For example, we have previously designed a peptide sequence comprised of two β-sheet-forming strands of alternating hydrophobic valine (V) and hydrophilic lysine (K) residues flanking a central valine-DPro-proline-threonine (−V^DPPT−) tetrapeptide sequence with a strong propensity to form a type II′ turn.[21] This sequence, previously labeled MAX1, undergoes an intramolecular folding event and adopts a β-hairpin conformation that subsequently self-assembles into β-sheet-rich hydrogels. The environmental stimuli by which peptide folding and consequent gelation occurs can be chosen by rationally modifying the various components of the peptide sequence including the hydrophobic residues, the polar residues, and the turn sequence. Specifically, stimuli of pH,[21] temperature,[22] and ionic strength[23] have been used to assemble gels through a controllable kinetic pathway leading to a desired ultimate stiffness. By removing the stimulus, such as changing the pH, the peptide unfolds and the gel becomes a solution, thus imparting reversibility to the system. In addition, the gels are responsive to mechanical stimuli; they can be shear thinned but quickly recover their initial viscoelastic properties after cessation of shear. The local morphology of these self-assembled, physical gels consists of a network of well-defined nanofibrils constructed by intermolecular assembly of amphiphilic β-hairpin peptides. Folded peptides are stabilized by a combination of intramolecular β-sheet hydrogen bonds between peptide strands, as well as van der Waals interactions between side chains. In the self-assembled state, the peptides have collapsed into a fibril by association of hydrophobic valine faces, thus defining the fibril cross section. The folded peptides assemble along the fibril axis by formation of intermolecular β-sheet hydrogen bonds between peptide backbones (Figure 1A). Interestingly, these filaments display exact cross sections and

(8) Lu, K.; Jacob, J.; Thiyagarajan, P.; Conticello, V. P.; Lynn, D. G. *J. Am. Chem. Soc.* **2003**, *125*, 6391−6393.
(9) Burkoth, T. S.; Benzinger, T. L. S.; Urban, V.; Morgan, D. M.; Gregory, D. M.; Thiyagarajan, P.; Botto, R. E.; Meredith, S. C.; Lynn, D. G. *J. Am. Chem. Soc.* **2000**, *122*, 7883−7889.
(10) Benzinger, T. L. S.; Gregory, D. M.; Burkoth, T. S.; Miller-Auer, H.; Lynn, D. G.; Botto, R. E.; Meredith, S. C. *Biochemistry* **2000**, *39*, 3491−3499.
(11) Collier, J. H.; Messersmith, P. B. *Adv. Mater.* **2004**, *16*, 907−910.
(12) Aggeli, A.; Bell, M.; Boden, N.; Carrick, L. M.; Strong, A. E. *Angew. Chem. Int. Ed.* **2003**, *42*, 5603−5606.
(13) Aggeli, A.; Bell, M.; Boden, N.; Keen, J. N.; Knowles, P. F.; McLeish, T. C. B.; Pitkeathly, M.; Radford, S. E. *Nature* **1997**, *386*, 259−262.
(14) Aggeli, A.; Nyrkova, I. A.; Bell, M.; Harding, R.; Carrick, L.; McLeish, T. C. B.; Semenov, A. N.; Boden, N. *Proc. Natl. Acad. Sci. U.S.A.* **2001**, *98*, 11857−11862.
(15) Marini, D. M.; Hwang, W.; Lauffenburger, D. A.; Zhang, S. G.; Kamm, R. D. *Nano Lett.* **2002**, *2*, 295−299.
(16) Lashuel, H. A.; LaBrenz, S. R.; Woo, L.; Serpell, L. C.; Kelly, J. W. *J. Am. Chem. Soc.* **2000**, *122*, 5262−5277.
(17) Behanna, H. A.; Donners, J.; Gordon, A. C.; Stupp, S. I. *J. Am. Chem. Soc.* **2005**, *127*, 1193−1200.
(18) Silva, G. A.; Czeisler, C.; Niece, K. L.; Beniash, E.; Harrington, D. A.; Kessler, J. A.; Stupp, S. I. *Science* **2004**, *303*, 1352−1355.
(19) Hartgerink, J. D.; Beniash, E.; Stupp, S. I. *Science* **2001**, *294*, 1684−1688.
(20) Sone, E. D.; Stupp, S. I. *J. Am. Chem. Soc.* **2004**, *126*, 12756−12757.
(21) Schneider, J. P.; Pochan, D. J.; Ozbas, B.; Rajagopal, K.; Pakstis, L.; Kretsinger, J. *J. Am. Chem. Soc.* **2002**, *124*, 15030−15037.
(22) Pochan, D. J.; Schneider, J. P.; Kretsinger, J.; Ozbas, B.; Rajagopal, K.; Haines, L. *J. Am. Chem. Soc.* **2003**, *125*, 11802−11803.
(23) Ozbas, B.; Kretsinger, J.; Rajagopal, K.; Schneider, J. P.; Pochan, D. J. *Macromolecules* **2004**, *37*, 7331−7337.

do not form higher order assemblies as demonstrated by cryo-TEM, small-angle neutron scattering,[24] and the optical transparency of the gels. This is in contrast to the higher order aggregates described as ribbons, bundles, and fibers[8,9,11,14−16] that have been reported in the literature thus far for amyloid and other β-sheet-forming peptide systems.

Herein we report the study of the supramolecular structure and self-assembly kinetics of a peptide in which intramolecular folding is designed against, but intermolecular β-sheet self-assembly can still occur. As described earlier, the central turn region of MAX1 contains the tetrapeptide sequence Val-^{D}Pro-Pro-Thr[21] that has a high propensity to adopt a type II′ turn due, in part, to the chirality of the ^{D}prolyl residue. However, when the ^{D}proline at the $i + 1$ position in the turn is replaced with the stereoisomer and naturally occurring amino acid ^{L}proline (Val-Pro-Pro-Thr), turn formation is strongly disfavored and intramolecular folding does not occur. This peptide instead adopts an extended β-strand conformation and assembles into hydrogen-bonded fibrils exhibiting a highly laminated, nontwisted morphology (Figure 1B). In addition, the self-assembled structure of these peptide fibrils is generally not reversible but stable under a wide range of temperature and pH, a property possessed by amyloid fibrils. Thus, nearly identical peptides, differing in the chirality of one amino acid, self-assemble via differing pathways into significantly different fibril morphologies and resultant materials.

We are interested in this current nonhairpin-forming peptide with the Val-Pro-Pro-Thr central peptide sequence because of its highly ordered, 2-D self-assembled nanostructure and the possibility of incorporating specific chemical functionality with regular arrangement on the nanoscale. Nearly all of the β-sheet fibrils reported in the literature thus far have an intrinsic helical pitch or twist that can vary depending on solution conditions and the degree of hierarchal assembly.[8,9,14−16] The peptide sequence described herein exhibits a nontwisted morphology under all conditions tested thus far and is believed to be the direct result of peptide sequence. We believe that the flat, nontwisted morphology and high stability of these quasi-crystalline structures is especially desirable for specific nano-applications where previous attempts using amyloid proteins, peptides, and viruses have been reported.[19,20,25−29] In addition, the ability to control the assembly process with temperature and pH may prove beneficial for potential nanotechnology.

Experimental Section

Peptide Synthesis. All the peptides were synthesized on Pal amide resin via automated Fmoc peptide synthesis employing an ABI 433A peptide synthesizer and HBTU/HOBT activation. The resulting dry resin-bound peptides were cleaved and side-chain-deprotected using a cocktail of TFA, thioanisole, ethanedithiol, and anisole in the ratio 90:5:3:2. Crude peptide was purified by RP-HPLC (preparative Vydac C18 peptide/protein column) employing a linear gradient from 12% to 100% B over 176 min, where solvent A is 0.1% TFA in water and solvent B is 90% acetonitrile, 10% water, and 0.1% TFA. After lyophilization, pure peptide was dissolved in water, resulting in a 100 μM solution, which was again lyophilized to ensure batch-to-batch consistency. The identity of the peptides was established by ESI mass spectrometry (see the Supporting Information).

For the purpose of this paper the peptide sequence VKVKVKVKV-PPTKVKVKVKV−NH_2 is designated as $(VK)_4$−VPPT−$(KV)_4$, the peptide sequence VKVKVKVKV^{D}PPTKVKVKVKV−NH_2 is designated as $(VK)_4$−V^{D}PPT−$(KV)_4$, and the peptide sequence VKVKVKVK-VKVKVKVKVK−NH_2 is designated as $(VK)_9$.

Procedure for Fibril Formation. Samples were prepared by dissolving lyophilized peptide in deionized water in small glass vials. An equal volume of pH 9 buffer solution (250 mM borate, 20 mM NaCl) was added to the dissolved peptide solution to obtain the final desired peptide concentration (1−10 mg/mL) and final buffer concentration of 125 mM borate, 10 mM NaCl, and pH 9. Vials were capped and allowed to incubate at room temperature for at least 2 weeks to over 6 months without agitation or stirring. Fibril formation could be qualitatively monitored by formation of precipitates in the vial. Incubation at elevated temperatures was achieved by placing the capped vials of solution in a VWR digital heat-block for a desired amount of time.

Circular Dichroism. CD spectra were collected on a Jasco J-810 spectropolarimeter. A 300 μM stock solution of the peptide was prepared and incubated in an ice bath along with buffer solutions (100 mM buffer and 20 mM NaCl). The buffers used were morpholine ethane sulfonate (MES at pH 6), bis−tris propane (BTP at pH 7 and 8), and borate (at pH 9 and 9.7) Prior to the start of an experiment, equal volumes (125 mL) of the peptide stock and buffer solutions were taken in a 1 mm path length quartz cell and gently mixed by inverting the cell a few times to yield a final concentration of 150 μM peptide, 50 mM buffer, and 10 mM NaCl. The cell was immediately placed in the instrument cell holder preequilibrated at 5 °C. Temperature-dependent wavelength scans were performed every 5 °C with a 10 min equilibration time at each temperature until 70 °C. For kinetic experiments, the sample was prepared by adding 125 μL of peptide solution (300 μM) to pH 9 buffer preequilibrated to the required temperature in the cell. Measurements were started immediately, and the CD signal was monitored at 216 nm every minute for 60 min. Concentrations of peptide solutions were determined by absorbance at 220 nm with the peptide extinction coefficient at 220 nm, $\epsilon_{220} = 15\,750\ \mathrm{cm^{-1}\,M^{-1}}$. Mean residue ellipticity $[\theta]$ was calculated from the equation $[\theta] = (\theta_{obs}/10lc)/r$, where θ_{obs} is the measured ellipticity in millidegrees, l is the length of the cell (centimeters), c is the concentration (molar), and r is the number of residues.

Infrared Spectroscopy. IR spectra were collected on a Nicolet Magna IR-860 spectrometer using a zinc selenide flow cell. The samples were prepared by dissolving the deuterated chloride salt of the peptide in D_2O to get a 1% (w/v) solution. To this solution an equal volume of pH 9 buffer (250 mM borate and 20 mM NaCl) in D_2O was added, and the contents were gently mixed and equilibrated on a sand bath at 50 °C. After equilibration, the samples were taken into the zinc selenide flow cell (100 μm path length) and spectra were recorded. The deuterated chloride salt of the peptide was prepared by lyophilizing the TFA salt of the peptide once in 0.2 M HCl and twice from D_2O.

Wide-Angle X-ray Scattering. X-ray diffraction patterns of dried peptide aggregates were collected at the National Synchrotron Light Source, Brookhaven National Laboratory, beamline X10A. Concentrated peptide solutions (10 mg/ml) were incubated in glass vials at 50 °C for 24 h. The ends of two small glass capillaries were drawn and then melted into small bulbs with a propane torch and then mounted onto a stretching apparatus. A small drop (2 μL) of peptide solution was placed between the ends of two small glass capillaries. The

(24) Ozbas, B.; Rajagopal, K.; Schneider, J. P.; Pochan, D. J. *Phys. Rev. Lett.* **2004**, *93*, 268106.
(25) Shenton, W.; Douglas, T.; Young, M.; Stubbs, G.; Mann, S. *Adv. Mater.* **1999**, *11*, 253−256.
(26) Scheibel, T.; Parthasarathy, R.; Sawicki, G.; Lin, X. M.; Jaeger, H.; Lindquist, S. L. *Proc. Natl. Acad. Sci. U.S.A.* **2003**, *100*, 4527−4532.
(27) Meegan, J. E.; Aggeli, A.; Boden, N.; Brydson, R.; Brown, A. P.; Carrick, L.; Brough, A. R.; Hussain, A.; Ansell, R. J. *Adv. Funct. Mater.* **2004**, *14*, 31−37.
(28) McMillan, R. A.; Paavola, C. D.; Howard, J.; Chan, S. L.; Zaluzec, N. J.; Trent, J. D. *Nat. Mater.* **2002**, *1*, 247−252.
(29) Mao, C.; Flynn, C. E.; Hayhurst, A.; Sweeney, R.; Qi, J.; Georgiou, G.; Iverson, B.; Belcher, A. M. *Proc. Natl. Acad. Sci. U.S.A.* **2003**, *100*, 6946−6951.

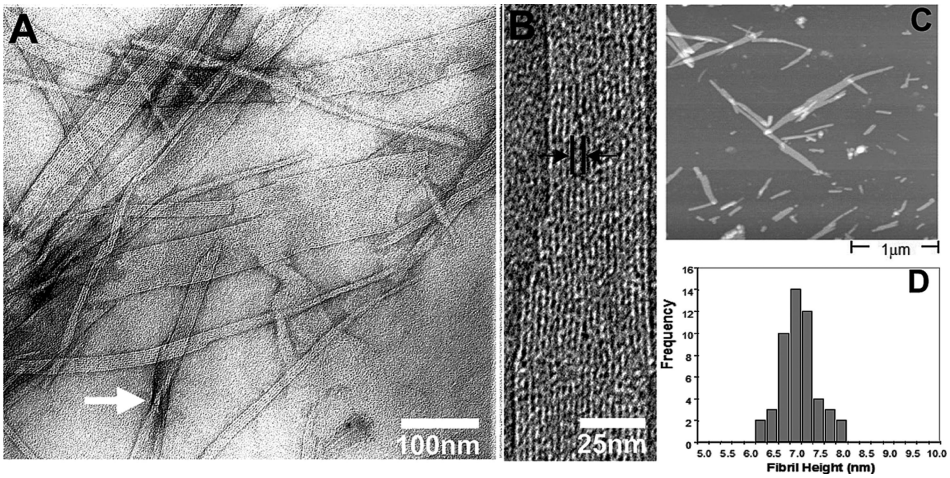

Figure 2. TEM micrographs of flat, ribbonlike $(VK)_4-VPPT-(KV)_4$ β-sheet fibrils negatively stained with uranyl acetate showing assembly in two dimensions. (A) Fibrils exceed lengths of 1 μm in the hydrogen-bonding direction and widths greater than 50 nm, sometimes folding over themselves as a random effect of fibril deposition onto the carbon film (white arrow). (B) High-magnification image of a fibril formed by the lateral association of 15−25 filaments, each ∼2.5 nm wide (black arrows). (C) AFM height image of $(VK)_4-VPPT-(KV)_4$ fibrils on a mica surface. (D) Frequency distribution of measured fibril height values with a mean of 7 ± 0.4 nm.

capillaries were slowly separated while keeping the solution between both ends. Drops of peptide were slowly added until a sufficiently long, dried stalk of fibrils was stuck to the end of one of the bulbs. The capillary was then mounted on an aluminum sample holder with a circular cutout and placed in the beam. Data were collected for 30 s with a Bruker 2-D CCD camera using monochromatic synchrotron X-rays ($\lambda = 1.54$ Å). Data for a blank sample holder with no capillary was collected and subtracted as background. The sample-to-detector distance was calibrated using silver behenate as a standard. Data analysis was performed using Bruker SAXS v3.324 software.

Transmission Electron Microscopy. A small volume (2−5 μL) of aged fibril solution was applied to carbon-coated copper grids. The samples were negatively stained by placing a drop of 2% (w/v) uranyl acetate aqueous solution on the grid. The excess of the solution was blotted with filter paper, and the sample was subsequently left to dry. Concentrated samples were diluted to ∼0.1% (w/v) with deionized water prior to staining. Bright field images of the fibril nanostructure were taken on a JEOL 2000-FX transmission electron microscope (TEM) at 200 kV accelerating voltage on both a Gatan CCD camera and Kodak negative films.

Atomic Force Microscopy. Aged peptide solutions were diluted to 0.01−0.1% (w/v) with deionized water, and 2−5 μL were applied to a freshly cleaved mica disk and allowed to dry. Some samples were rinsed with ∼150 μL of deionized water to remove dried salt and unbound peptide. Samples were imaged on a Digital Instruments Multi Mode Nanoscope IIIA atomic force microscope (AFM) in tapping mode using silicon tips (300 kHz, 40 N/m) with a scan rate of 0.75−1.25 Hz. Digital Instruments software was used to measure the height of the fibrils using the Section Analysis feature. The measurements were compiled and the statistical mean and standard deviation of fibril height were calculated.

Results

Peptide Design. The general design motif of $(VK)_4-VPPT-(KV)_4$ consists of two β-sheet-forming strands flanking a central tetrapeptide turn sequence. The strands are composed of alternating hydrophobic V and hydrophilic K residues, a motif that has been shown to favor β-sheet formation[30,31] (see Figure 1). We have selected valine as the hydrophobic residue due to its high β-sheet propensity and lysine as the hydrophilic group due to its positively charged side chains in neutral aqueous solution that impart solubility to the peptide. The central region consists of the tetrapeptide sequence of Val-Pro-Pro-Thr. Crystallization of Pro-Pro dipeptides has previously shown that the ^{L}Pro-^{L}Pro sequence favors a *trans*-prolyl linkage and an open conformation in the solid state.[32−34] Furthermore, inclusion of a β-branched valine residue preceding the first proline residue has been shown to enforce a *trans*-prolyl linkage due to the steric constraints of the proline side chain.[35,36] Both the current experimental data and previous examples from the literature show that the designed peptide maintains all trans linkages thereby adopting an extended β-strand conformation when self-assembled. Therefore, the height of a β-sheet filament or hierarchal stack should exhibit a height dictated by the extended length of the peptide.

Structural Characterization. Fibril formation of $(VK)_4-VPPT-(KV)_4$ occurs at pH 9.0 and room temperature over a period of at least 2 weeks forming a solution with visible precipitates. Figure 2A shows representative TEM images of an aged fibril solution of which a drop was deposited on a carbon-coated copper grid and negatively stained with uranyl acetate. Fibrils assembled to lengths well over 1 μm and exhibit widths on the order of 10−100 nm. Closer examination of a fibril reveals that each fibril is composed of smaller fibrillar subunits we designate as filaments. Filaments are ∼2.5 nm wide and laterally associated into stacks of greater than 50 filaments to produce flat, nontwisted fibrils. Although fibrils can sometimes be seen to fold over on themselves (see Figure 2A), the lack of regular twisting indicates that any twist observed with TEM is a random effect of these long ribbonlike fibrils being deposited on a surface from solution. The negative stain can be seen to deposit not only at the edges of the fibrils, but also between filaments, as is evident by the dark lines along the fibril axis in Figure 2B. These striations, not evident in unstained samples, are the result of negative stain depositing either

(30) Brack, A.; Caille, A. *Int. J. Pept. Protein Res.* **1978**, *11*, 128−139.
(31) Brack, A.; Orgel, L. E. *Nature* **1975**, *256*, 383−387.
(32) Aubry, A.; Vitoux, B.; Marraud, M. *Biopolymers* **1985**, *24*, 1089−1100.
(33) Balaram, H.; Prasad, B. V. V.; Balaram, P. *J. Am. Chem. Soc.* **1983**, *105*, 4065−4071.
(34) Benedetti, E.; Bavoso, A.; Diblasio, B.; Pavone, V.; Pedone, C.; Toniolo, C.; Bonora, G. M. *Biopolymers* **1983**, *22*, 305−317.
(35) Grathwohl, C.; Wuthrich, K. *Biopolymers* **1976**, *15*, 2025−2041.
(36) Reimer, U.; Scherer, G.; Drewello, M.; Kruber, S.; Schutkowski, M.; Fischer, G. *J. Mol. Biol.* **1998**, *279*, 449−460.

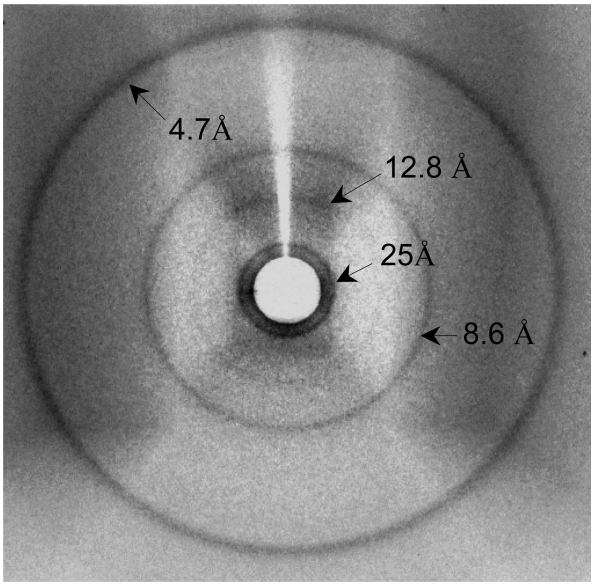

Figure 3. 2-D X-ray diffraction pattern of dried $(VK)_4-VPPT-(KV)_4$ fibrils with reflections occurring at 25, 12.8, 8.6, and 4.7 Å. The bright cone on the top of the meridian is a shadow from the capillary mounted on the sample holder. The sample holder itself also appears as a slight shadow in the pattern.

between filaments in relatively hydrophilic regions (e.g., rich in lysine as opposed to valine) or in small grooves on the surface of the fibril.

Tapping mode atomic force microscopy of the fibrils reveals a similar general morphology of flat, ribbonlike structures lacking any regular twist (Figure 2C). However, individual filaments cannot be discerned due to the fact that in TEM individual filament visualization is possible due to the variation of the electron density across the width of a fibril, especially when stained; the height across the fibril may not vary enough to be detected by an AFM tip with a radius (5−10 nm) the size of two or more filament diameters (2.5 nm each). However, the average height across each fibril (relative to the mica surface) is consistently 7 ± 0.4 nm (Figure 2D), independent of the width of the fibril and, therefore, the number of stacked filaments. The combination of microscopy data leads to the conclusion that each filament has finite dimensions of 7 nm in height and a characteristic width of ~2.5 nm as revealed by AFM and TEM, respectively.

X-ray diffraction of dried $(VK)_4-VPPT-(KV)_4$ peptide fibrils was obtained using a method designed to align amyloid fibrils for oriented fiber diffraction (see the Experimental Section). Figure 3 shows the resulting 2-D diffraction pattern. While significant fibril orientation was not observed, small- and wide-angle reflections were observed that are consistent with TEM observations. First, a strong reflection was observed corresponding to a *d* spacing of 25 Å, a value that correlates well with the filament diameter as observed by TEM. Second, two other reflections were observed corresponding to *d* spacings of 12.8 Å and 8.6 Å commensurate with what is expected for the second and third-order reflections of the 25 Å long spacing (d_1:d_2:d_3 = d_1:$d_1/2$:$d_1/3$ for a layered system). Third, a strong reflection corresponding to a *d* spacing of 4.7 Å was observed. This reflection is reported for nearly all amyloid and peptide β-sheet fibrils and is considered to be a β-sheet signature corresponding to the distance between hydrogen-bonded peptides along the fibril axis.[7] X-ray diffraction of a similar polypeptide, poly(Val-Lys), has been previously reported and was indexed with comparable results.[37]

Structural Model. The proposed structural model and hierarchy of assembly is illustrated in Figure 4. The β-sheet formation stabilized by intermolecular hydrogen bonding between peptide backbones drives growth along the fibril axis to over micrometers in length. The peptide backbone, therefore, is transverse to the fibril axis, a structure often described as "cross-β" in amyloid fibrils. AFM reveals that the height of each fibril normal to both the fibril axis and the lamination direction is 7 nm. This is the expected length of the $(VK)_4-VPPT-(KV)_4$ peptide in an extended β-strand conformation when measured from N to C terminus (20 residues × 3.5 Å per residue = 7 nm). It follows that the width of each filament in the lamination direction must be defined by the length of the side chains of the peptide and the stacking of β-sheets. With TEM, the width of the filaments was measured as 2.5 nm. This dimension is consistent with the expected width of two β-sheets stacked in the direction transverse to both the fibril axis and the peptide backbone (see Figure 4). The alternating, amphiphilic peptide sequence in combination with hydrophobic effects should favor polar β-sheets in which all valine side chains are on one side of the sheet and lysines are on the opposing side. Two polar β-sheets could then form a stable bilayer, which we designate as a filament, via hydrophobic collapse of the valine faces. Thus, the 2.5 nm wide filament visualized by TEM consists of a valine-rich hydrophobic core and a lysine-rich outer shell. Lateral association of filaments, therefore, must occur by packing of lysine faces. Under these solution conditions of pH 9 and 10 mM NaCl, a sufficient amount of lysine side chains must be deprotonated and/or screened to overcome the otherwise electrostatic repulsion between filaments. A laminated fibril, therefore, consists of alternating layers of valine and lysine as a result of filament formation and lateral association, respectively. The X-ray diffraction data further support this with the strong reflection observed corresponding to a long *d* spacing of 2.5 nm for $(VK)_4-VPPT-(KV)_4$ fibrils. The intersheet spacings in β-sheet fibrils of neat poly(valine) and of neat poly(lysine) as determined by X-ray diffraction have been previously reported as 9.5 Å and 14.6 Å, respectively.[38,39] For the proposed bilayer model, the periodicity, and fibril diameter, is expected to be equal to the sum of a valine and a lysine intersheet spacing (9.5 Å + 14.6 Å = 24.1 Å) Again, this is consistent with our observed fibril diameter and the X-ray diffraction data of 2.5 nm. The stacking of polar β-sheets has been described for silklike polypeptides in which glycine and alanine faces pack in similar fashion.[40] Furthermore, previous work by Brack and Orgel, who studied poly(Val-Lys) as well as other polypeptides composed of alternating hydrophobic and hydrophilic residues, proposed that such polymers would form "stacked bilayers" in which β-sheets pack by association of like faces, i.e., valine to valine and lysine to lysine.[31] X-ray diffraction of oriented poly(Val-Lys) and other alternating polypeptide crystallites supported their stacked bilayer hypothesis[37] though, to the best of our

(37) Vives, J.; Azorin, F.; Subirana, J. A.; Brack, A.; Mayer, R. *Biopolymers* **1985**, *24*, 1801−1808.
(38) Komoto, T.; Kim, K. Y.; Oya, M.; Kawai, T. *Makromol. Chem. Macromol. Chem. Phys.* **1974**, *175*, 283−299.
(39) Fandrich, M.; Dobson, C. M. *EMBO J.* **2002**, *21*, 5682−5690.
(40) Krejchi, M. T.; Cooper, S. J.; Deguchi, Y.; Atkins, E. D. T.; Fournier, M. J.; Mason, T. L.; Tirrell, D. A. *Macromolecules* **1997**, *30*, 5012−5024.

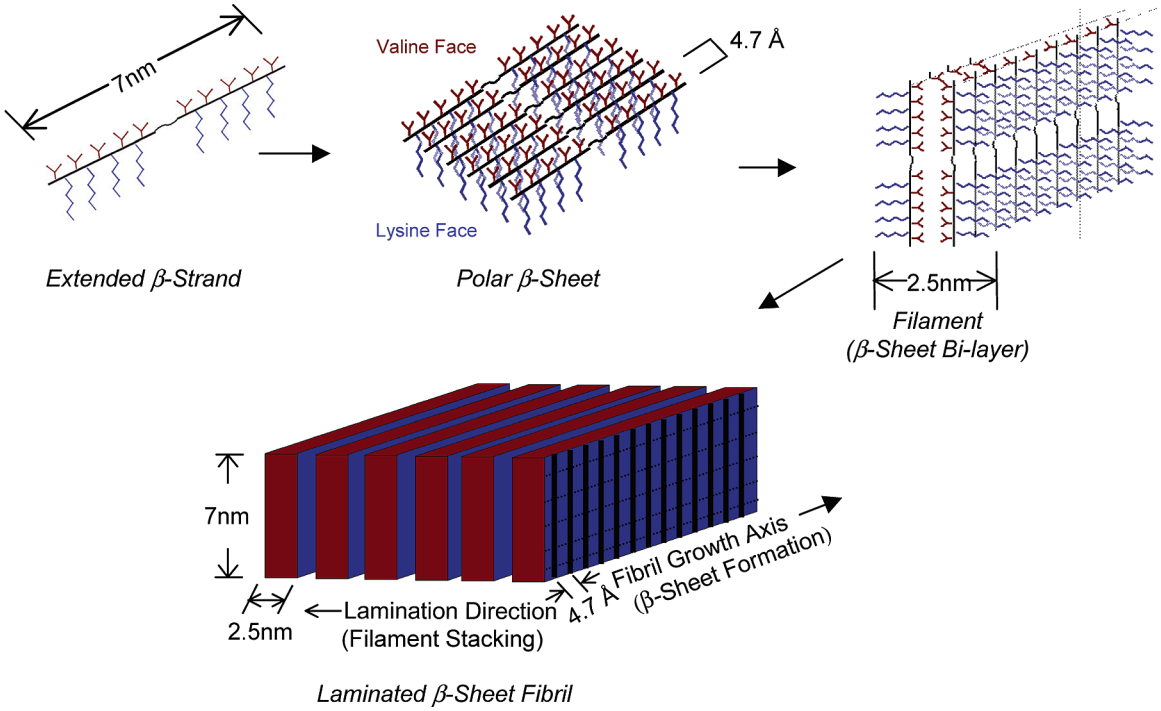

Figure 4. Hierarchal assembly of peptides into a β-sheet fibril. Peptides in an extended β-strand conformation assemble into polar β-sheets with distinct hydrophobic (valine) and hydrophilic (lysine) faces. β-sheets collapse into a filament (bilayer) by packing of hydrophobic faces. Filaments stack laterally into laminated β-sheet fibrils.

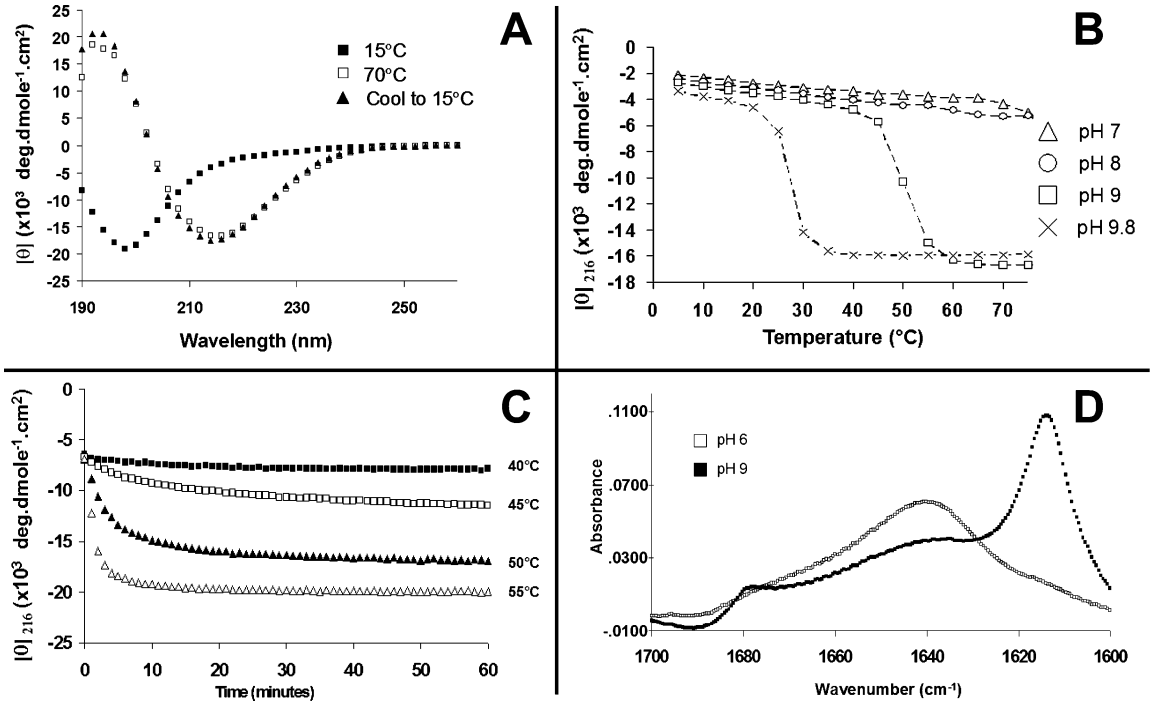

Figure 5. (A) CD spectroscopy of a 150 μM $(VK)_4-VPPT-(KV)_4$ solution at pH 9 showing the transition from random coil at 15 °C (■) to β-sheet at 70 °C (□) and maintained to 15 °C (▲). (B) Mean residue ellipticity at $\lambda = 216$ nm showing β-sheet transition vs temperature for pH 7 (△), pH 8 (○), pH 9 (□), and pH 9.8 (×) peptide solutions. (C) Mean residue ellipticity at $\lambda = 216$ nm showing β-sheet formation vs time for 40 °C (■), 45 °C (□), 50 °C (▲), and 55 °C (△). (D) Fourier transform infrared spectroscopy revealing the transformation from a random coil conformation in unbuffered ~pH 6 solution (□) to a β-sheet conformation at pH 9 (■) when incubated for 5 h at 50 °C. IR spectra in the amide I′ region at pH 9 show a strong absorption at 1615 cm^{-1} and a weak absorption at 1680 cm^{-1}, generally associated with an antiparallel arrangement.

knowledge, direct visualization of these structures by TEM and AFM has not previously been reported.

Self-Assembly Kinetics. Initial studies of the $(VK)_4-VPPT-(KV)_4$ peptide were conducted at room temperature where β-sheet formation, and thus fibril formation, takes over 2 weeks. However, it was discovered that fibril formation could be accelerated by incubation at elevated temperatures. Figure 5A shows a plot of mean residue ellipticity versus wavelength for a $(VK)_4-VPPT-(KV)_4$ sample at pH 9 that was heated from 15 to 70 °C and then cooled to 15 °C. Wavelength scans at

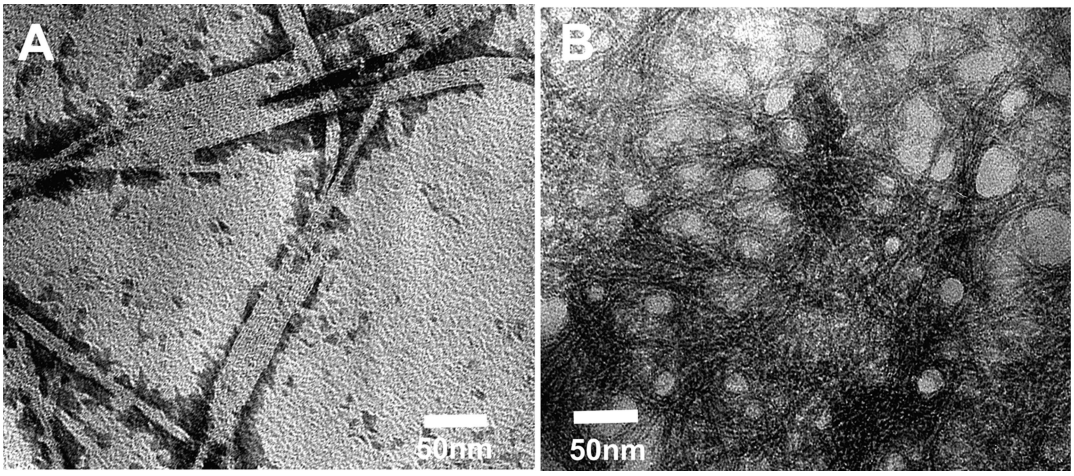

Figure 6. Negatively stained $(VK)_4-VPPT-(KV)_4$ fibrils grown at (A) 50 °C and (B) 70 °C.

each of the three temperatures shows a transition from random coil to β-sheet as the temperature is increased from 15 to 70 °C. The peptide maintains its β-sheet conformation, even when cooled back to 15 °C, indicating an irreversible conformational transition with temperature. Similarly, plotting the mean residue ellipticity values at a wavelength of $\lambda = 216$ nm while increasing temperature shows that a significant transition to β-sheet occurs at around 50 °C for pH 9 solutions (Figure 5B). The rate of β-sheet formation increases with increasing temperature and can vary from days to weeks at room temperature to an hour at 50 °C to within seconds at 70 °C. Figure 5C shows a plot of mean residue ellipticity at $\lambda = 216$ nm versus time for selected temperatures demonstrating the effect of temperature on rate of β-sheet formation. FT-IR analysis of the amide I′ band of an unbuffered $(VK)_4-VPPT-(KV)_4$ solution, approximately pH 6, incubated at 50 °C for 5 h shows a random coil spectrum as compared to a solution incubated at pH 9 and 50 °C for 5 h in which the spectrum is predominately β-sheet as demonstrated by a characteristic peak at 1615 cm^{-1} and a shoulder at 1680 cm^{-1} (often associated with an antiparallel β-sheet arrangement[41]) (Figure 5D). TEM and AFM of solutions incubated at elevated temperatures reveal the same nontwisted, laminated morphology and the same 7 nm height of the fibrils as was found for fibrils grown slowly at room temperatures (Figure 6A). Thus, the peptide maintains its extended conformation and assembles into morphologically similar fibrils at higher temperatures, though the rate of assembly is faster.

As the temperature is increased to over 70 °C, fibril formation occurs in a matter of seconds, and concentrated peptide solutions (10 mg/mL) become brittle gels (Figure 6B). Fibrils grown under these conditions exhibit considerably less lamination, which affords more flexible fibrils, capable of entanglement and, thus, gelation. Dynamic oscillatory rheological measurements of gels constructed at elevated temperatures show linear viscoelastic behavior for strain values only to ~0.2% (data not shown) as compared to gels formed by the $(VK)_4-V^DPPT-(KV)_4$ peptide[21] that exhibit linear viscoelastic behavior up to 20% strain. $(VK)_4-VPPT-(KV)_4$ gels, though rigid ($G' > 1$ kPa), can easily be broken by a small amount of strain and do not recover, making them unsuitable for many hydrogel applications, whereas $(VK)_4-V^DPPT-(KV)_4$ gels fully recover once strained beyond the linear strain limit.[21]

In addition to temperature, β-sheet formation can be modulated by the pH of the solution and peptide concentration. Figure 5B shows the effect of pH on the random coil to β-sheet transition. At pH 8 and less, the peptide remains as random coil up to 70 °C. As the pH is increased, the transition shifts to around 52 °C at pH 9 and 27 °C at pH 9.8. Concentrated peptide solution (10 mg/ml) incubated at pH 9.8 and room temperature forms β-sheet within seconds, but no gel is formed. Rather, a cloudy precipitate forms composed of fibril flocculates. Thus, the rate of β-sheet formation is not the only factor in governing gelation as is evident by similar rates of β-sheet formation at pH 9 and 70 °C versus pH 9.8 and room temperature with gelation only occurring in the former condition. This is likely due to the decreasing solubility of the fibrils as the pH is increased. The dependence of the coil−β-sheet transition temperature on pH implicitly exhibits the roles of hydrophobic interactions and electrostatics in the assembly of the peptide. At pH less than 8, the peptide does not assemble even at high temperatures due to electrostatic repulsions between lysine side chains despite increasing hydrophobic effect with increasing temperature. But, as the pH is increased and the ϵ-amino groups of the lysine side chains are progressively deprotonated, the transition temperature shifts to lower temperatures. As the pH is increased above 10, the peptide is no longer soluble.

Discussion

To understand the mechanism of fibril formation, we analyzed the structure of $(VK)_4-VPPT-(KV)_4$ fibrils formed at temperatures of 70 °C and pH 9 that display a fibril morphology of minimal lamination, i.e., 1−3 filaments per fibril as compared to fibrils incubated at room temperature for periods exceeding 1 month where fibril lamination is maximum. These structural differences may be due to a nucleation and growth mechanism of fibril formation often reported for amyloid proteins.[42] As the temperature is increased above 70 °C, many fibrils nucleate concurrently resulting in an entangled network of thin fibrils, whereas at room temperature, fibril nucleation is slow and free peptide in solution joins already nucleated fibrils resulting in

(41) Jackson, M.; Mantsch, H. H. *Crit. Rev. Biochem. Mol. Biol.* **1995**, *30*, 95−120.

(42) Lomakin, A.; Teplow, D. B.; Kirschner, D. A.; Benedek, G. B. *Proc. Natl. Acad. Sci. U.S.A.* **1997**, *94*, 7942−7947.

very large fibril stacks that slowly precipitate over the course of days to months. It would seem that one could control the size of the fibrils by controlling the temperature and thus the rate of nucleation and growth. This hypothesis is partially substantiated as TEM analysis of fibril solutions incubated at 70 °C shows predominately thin fibrils of minimal lamination (Figure 6B). However, due to aggregation and possible effects of sample preparation such as drying, initially thin fibrils are sometimes seen to stack into wider laminates. This indicates that the growth of fibrils in the lamination direction can occur by two mechanisms, namely, the addition of free peptide to a growing fibril as well as the coarsening of fibrils by aggregation and stacking of already nucleated filaments. This second mechanism of fibril growth via aggregation has been previously described for a monomeric variant of transthyretin in which the fibrillization is considered an energetically "downhill polymerization" as opposed to classic nucleation and growth process where the nucleus is the highest energy species.[43]

Nyrkova et al. have developed a hierarchal model regarding the structural morphology of peptide based fibrils.[44] The model is based on the premise that, because the structural units of a peptide are chiral, the peptide itself can be approximated as a chiral rodlike monomer. Rods assemble into twisted and bent β-sheets with two chemically distinct faces. The sheets are driven to assemble into twisted bilayers, a.k.a. ribbons or filaments, by favorable side chain interactions, generally hydrophobic in nature. Assembly of sheets into ribbons and higher order twisted structures is impeded by the elastic penalty of untwisting the sheets from their natural state, a process necessary to accommodate more sheets in an assembly. Thus, for specific peptide concentrations and energies of interaction, there is an optimal amount of sheets that will assemble when the energies of attraction are balanced by the elastic costs of untwisting. The result is a twisted structure with a specific amount of assembled sheets and overall twist. However, when the energies of attraction between filaments is sufficiently high or if the peptide monomer is not twisted, the model predicts that the ribbons will be untwisted and will assemble into "infinite stacks" where there is no limit to the amount of sheets that can assemble in the lateral direction. The $(VK)_4-VPPT-(KV)_4$ peptide seems to fit this latter condition as is evident by the highly laminated, nontwisted fibrils visualized by TEM and AFM. In Nyrkova's model, the predicted twist is calculated by minimization of an equation defined by the geometrical parameters of the sheet as well as the energy of interaction between sheets. We hypothesize that the origin of the highly stacked morphology for $(VK)_4-VPPT-(KV)_4$ is primarily due to the conformation of the peptide, as opposed to an extraordinarily strong interaction between filaments. The morphology of fibrils nucleated and grown at low temperature versus high temperature are all untwisted and only vary in the extent of lamination due to different rates of assembly. If the $(VK)_4-VPPT-(KV)_4$ fibrils followed the behavior predicted by Nyrkova, the less laminated fibrils assembled at higher temperatures would exhibit twisting. Our hypothesis is that the fibrils are not twisted because the filaments are not twisted. And, the filaments are not twisted because the central proline residues interrupt the natural twist of the peptide. Thus, the approximation of the peptide as a chiral, rodlike monomer my not hold in this case. A better view of the peptide would be to see it as two distinct, chiral rodlike monomers, each with its own tendency for twisting, covalently linked by two proline residues. In fact, it is well-known that proline can serve as a "β-sheet breaker" in natural proteins[45] as may well be the case for this peptide. To test our hypothesis as to the role of proline in fibril lamination, we synthesized an 18 amino acid peptide consisting only of alternating valine and lysines residues, $(VK)_9$. Assembly of this peptide under identical conditions as those for $(VK)_4-VPPT-(KV)_4$ in Figure 2 (pH 9, room temperature for over 2 weeks) produced a precipitated solution of β-sheet fibrillar aggregates as demonstrated by CD spectroscopy and electron microscopy. TEM analysis of the fibrils reveals a highly twisted fibril morphology with 6.5 nm filament diameters, approximately equal to the expected length of an 18 amino acid peptide in an extended conformation (Figure 7). This strongly suggests that the origin of the nontwisted conformation is a result of the central Pro-Pro region.

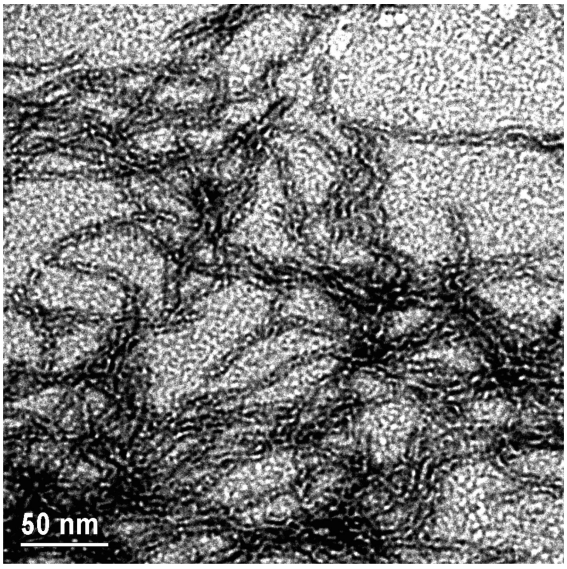

Figure 7. Negatively stained fibrils of $(VK)_9$ exhibiting a twisted-bundle morphology.

Conclusion

Peptides have been designed consisting of two β-sheet-forming arms containing alternating valine and lysine residues flanking a central diproline sequence that adopt an extended β-strand conformation and assemble into β-sheet-rich, amyloid-like fibrils by lateral assembly of individual filaments. Filaments are 2.5 nm in width and exactly the length of one extended peptide in height, ~7 nm. The fibrils exceed micrometers in length and over 50 nm in width. The fibrils are not twisted and are characterized by a stacked bilayer model in which β-sheets pack by association of like faces (valine to valine and lysine to lysine). The rate of self-assembly and the resulting degree of fibril lamination can be tuned by adjusting either the pH or temperature. The laminated morphology of the $(VK)_4-VPPT-(KV)_4$ peptide is likely an effect of the central ^{L}Pro-^{L}Pro sequence. This hypothesis will lead to the design of new peptides with the intent of gaining further insight as to the relationship

(43) Hurshman, A. R.; White, J. T.; Powers, E. T.; Kelly, J. W. *Biochemistry* **2004**, *43*, 7365−7381.
(44) Nyrkova, I. A.; Semenov, A. N.; Aggeli, A.; Boden, N. *Eur. Phys. J. B* **2000**, *17*, 481−497.
(45) Chou, P. Y.; Fasman, G. D. *Annu. Rev. Biochem.* **1978**, *17*, 251−276.

between the peptide sequence and self-assembled β-sheet morphology so as to effectively design new functional materials.

Acknowledgment. The authors acknowledge financial support from the National Institutes of Health Grant 1-P20-RR17716-01, NSF IGERT Fellowship DGE-0221651, NSF Career Award DMR-0348147, and NSF Career Award CHE-0348323. Use of the National Synchrotron Light Source, Brookhaven National Laboratory, was supported by the U.S. Department of Energy, Office of Science, Office of Basic Energy Sciences, under Contract No. DE-AC02-98CH10886. We acknowledge the W.M. Keck foundation for partial funding of the College of Engineering Electron Microscopy Lab at the University of Delaware and Dr. K. H. Gardner for thoughtful discussions.

Supporting Information Available: Experimental procedures including mass spectra of the purified peptide. This material is available free of charge via the Internet at http://pubs.acs.org.

JA054721F